# Tear proteomics of orbital decompression for disfiguring exophthalmos in inactive thyroid-associated ophthalmopathy

LIHONG JIANG[1,2], AO RONG[1], RUILI WEI[3], JIALE DIAO[3], HUI DING[2] and WEI WANG[2]

[1]Department of Ophthalmology, Tongji Hospital, School of Medicine, Tongji University, Shanghai 200065;
[2]Department of Ophthalmology, Zhabei Central Hospital, Jingan District, Shanghai 200070;
[3]Department of Ophthalmology, Changzheng Hospital, Naval Medicine University, Shanghai 200003, P.R. China

Received November 15, 2019; Accepted July 20, 2020

DOI: 10.3892/etm.2020.9383

**Abstract.** The progress and achievements that have been made in tear proteomics in thyroid-associated ophthalmopathy (TAO) are critical for exploring the pathogenesis of TAO and investigating potential therapeutic targets. However, the tear proteomics of orbital decompression for disfiguring exophthalmos in inactive TAO have yet to be properly investigated. In the present study, orbital decompression was performed to repair disfiguring exophthalmos in patients with inactive TAO. Tears were collected before and after orbital decompression in patients with inactive TAO. Liquid chromatography with tandem mass spectrometry (LC-MS/MS) was performed to explore the changes in tear proteomics. Bioinformatics analyses were then employed to analyze the functions of the differentially expressed proteins (DEPs) identified by LC-MS/MS. The palpebral fissure height and exophthalmia area were significantly restored after 1 month of orbital decompression such that they approached the normal levels identified in healthy eyeballs. Among the 669 proteins identified by LC-MS/MS, 83 proteins were changed significantly between the preoperative and postoperative stages in inactive TAO patients and healthy control individuals. The DEPs were predicted to be involved in numerous signaling pathways. Bioinformatics analyses revealed that pathways associated with the immune system, metabolism, programmed cell death, vesicle-mediated transport, neuronal system and extracellular matrix organization may fulfill significant roles in orbital decompression in patients with inactive TAO. Taken together, these results provided a preliminary understanding of the mechanism of orbital decompression for disfiguring exophthalmos in inactive TAO patients.

*Correspondence to:* Professor Ao Rong, Department of Ophthalmology, Tongji Hospital, School of Medicine, Tongji University, 389 Xin Cun Road, Shanghai 200065, P.R. China
E-mail: rongao893@163.com

*Abbreviations:* DEPs, differentially expressed proteins; GO, Gene Ontology; BP, biological process; CC, cellular component; MF, molecular function; IGF, insulin-like growth factor; REAC, Reactome; TAO, thyroid-associated ophthalmopathy

*Key words:* tear proteomics, inactive thyroid-associated ophthalmopathy, orbital decompression, bioinformatics analysis

## Introduction

Exophthalmos, which is one of the most serious symptoms of thyroid-associated ophthalmopathy (TAO), leads to a marked decrease in the quality of life of patients with TAO (1). Although methylprednisolone pulse therapy decreases extraocular muscle enlargement, it does not change orbital fat volume or exophthalmos (2,3). Orbital fat decompression surgery is effective for the treatment of exophthalmos (4). Orbital decompression, which was first described by Krönlein in 1889 (5), is commonly performed for disfiguring exophthalmos, congestion and optic neuropathy in patients with TAO (6). Although a small percentage of patients require repeat surgery, one round of decompression surgery can ameliorate exophthalmos in inactive TAO cases (7). Although the majority of the published literature on orbital decompression is comprised of retrospective studies, evidence from these investigations has indicated that removal of the medial and lateral wall, and deep lateral wall decompression are probably the most effective surgical methods (8). Inflammation of orbital tissue leads to an increase in the mass of extraocular muscles and orbital fat, and eventually leads to an increase in retrobulbar pressure (9). When the fixed space of the skeletal orbit cannot contain the enlarged tissue, exophthalmos inevitably occurs. It becomes more serious when eyeball congestion or other factors cause the enlargement of the eyeball volume. Orbital decompression seems to straightforwardly eliminate this extra unnecessary pressure, thus ameliorating exophthalmos (10). In addition to eliminating inflammation caused by stress, it remains unknown, however, whether decompression leads to changes in other signaling pathways.

Tear tests have fulfilled an increasingly critical role in the diagnosis and management of ocular surface diseases, due to their noninvasive nature (11). As bodily fluids, tears, similar to urine and blood, reflect the development and progression of certain diseases, including cancer and diabetes (12). Under physiological conditions, the majority of human tear proteins, such as lysozyme, lactoferrin and soluble immunoglobulin A,

come from the lacrimal gland, the tarsal gland, and the paralacrimal gland (13). Small amounts of proteins are derived from release by blood vessels, cells or tissues on the surface of the eye (14). However, when the conjunctiva is stimulated abnormally, the protein overflow from the ocular surface vessels changes significantly (15). Previous studies have confirmed that numerous proteins are changed significantly in the tears of patients with TAO compared with in tears from healthy individuals (16,17). For example, α-1-antichymotrypsin, cystatin-C, interleukin (IL)-1β and IL-6 were upregulated, whereas phospholipase $A_2$, STAT1-α/β, abhydrolase domain containing 14B and S100A4 were downregulated in patients with TAO (9,18-21). Additionally, some tear proteins exhibited different types of change when comparing the active and inactive stages of TAO. For example, IL-7 was reduced in tears from patients with active TAO, whereas its levels were increased in tears from patients with inactive TAO, when both were compared with those found in tears from healthy individuals (22). Previous studies (16-22) on the tear proteomics of TAO have mostly focused on active or mixed-status patients, and tear proteomics in TAO cases in the inactive stage have yet to be properly investigated. In addition, changes in tear proteomics before and after orbital decompression surgery have yet to be studied. Therefore, revealing the changes in tear proteomics and clarifying the mechanism of orbital decompression for disfiguring exophthalmos in patients with inactive TAO has become an increasingly urgent clinical issue. The present study aimed to identify abnormal changes in tear proteins, and to explore the potential enrichment of signaling pathways, and their interactions between the preoperative and postoperative stages of orbital decompression, in patients with inactive TAO using liquid chromatography with tandem mass spectrometry (LC-MS/MS) and bioinformatics analyses.

## Materials and methods

*Patients*. Patients with inactive TAO and unilateral exophthalmos (3 males and 3 females; average age, 46.7±6.3; age range, 44-58 years) with a clinical activity score (CAS) <3 (1.7±0.5) were collected and selected from the Department of Ophthalmology, Zhabei Central Hospital between November 2017 and August 2018. Thyroid hormones and associated antibodies of these cases were found to be within the normal range. Six age-matched healthy cases (2 males and 4 females; average age, 50.2±5.4; age range, 37-53 years) were selected as healthy control subjects. In the present study, all participants provided written informed consent, and all protocols were approved by the Ethics Committee of Zhabei District Central Hospital.

*Chemicals*. Trypsin was purchased from Promega Corporation. Dithiothreitol, formic acid, iodoacetamide, ammonium bicarbonate ($NH_4HCO_3$) and trifluoroacetic acid were obtained from Sinopharm Chemical Reagent Co., Ltd.. High-performance liquid chromatography (HPLC)-grade acetonitrile (CAN) was acquired from Thermo Fisher Scientific, Inc. Synthetic indexed retention time (SiRT) peptides were obtained from Biognosys AG. The other chemicals were purchased from Sigma-Aldrich (Merck KGaA), unless otherwise indicated.

*Palpebral fissure determination*. The palpebral fissure was calculated through three-dimensional (3D) reconstruction of orbital computed tomography (CT) obtained from a 128-slice spiral CT (Philips Brilliance 64; Philips Medical Systems, Inc.) using matching Mimics software v5.0.2.10010 (Materialise NV). The measurement parameters and methods followed were identical to those described previously (23). The scan images were processed using Mimics software. All multiplanar (coronal and sagittal) images and 3D-reconstructed images were displayed at the bone window on the basis of the original horizontal sections. Surface reconstruction of whole orbital content was generated with 3D semi-automatic segmentation. Anatomic landmarks of the orbit were located on the 3D model of the orbit, and the relevant length measurements were calculated using the aforementioned Mimics software. All data were collected by the same technician, and the average value of the same parameter was taken after three measurements to reduce measurement error.

*Ocular surface disease index (OSDI) score*. The OSDI score was calculated as described previously according to an OSDI questionnaire survey (24).

*Tear collection and preparation*. Tears were collected the day before the orbital decompression surgery and 1 month after the surgery. Tear collection was carried out as previously described (25). Briefly, tear samples were collected with a 10-$\mu$l capillary glass tube from the eyelid conjunctival sac, not touching the ocular surface and without application of any local drug. All tears were stored in a -80˚C freezer prior to analysis.

Tears were diluted with 50 mM $NH_4HCO_3$ and centrifuged thrice for 20 min at 14,000 x g at 20˚C in YM-10 filter units. Mixed protein lysates were reduced for 1 h at room temperature by addition of a final concentration of 10 mM dithiothreitol, and then alkylated for 1 h at room temperature in the dark by the addition of a final concentration of 55 mM iodoacetamide. The solvent of the protein mixtures was exchanged with 50 mM $NH_4HCO_3$ by centrifugation for 20 min at 14,000 x g at 20˚C for 3 times, followed by protein digestion with sequencing grade-modified trypsin at a protein-to-enzyme ratio of 50:1 at 37˚C overnight. Tryptic peptides were collected by centrifugation for 20 min at 14,000 x g at 20˚C. The tryptic peptides were treated with 1% trifluoroacetic acid (TFA), and subsequently purified using C18 Ziptips, eluted with 0.1% TFA in 50-70% ACN. The eluted peptides were lyophilized using a Savant™ SpeedVac™ (Thermo Fisher Scientific, Inc.) and resuspended in 1% formic acid/5% ACN. The SiRT peptides were spiked into the sample prior to analysis, according to the manufacturer's instructions.

*High pH reversed-phase fractionation*. The pooled tears were further fractionated using high pH reversed-phase chromatography for building each spectral library. The pooled digests were lyophilized using a Savant SpeedVac, and resuspended in 5% ACN in 0.05 M ammonium formate. The digested peptides (500 $\mu$g) were fractionated using high pH reversed-phase separation on a Dionex® Ultra-HPLC system (Thermo Fisher Scientific, Inc.) with a 2.1x150 mm Ethylene Bridged Hybrid (BEH) C18 3-$\mu$m column (Waters Corporation) at 40˚C with

0.2 ml/min flow and a 60 min ACN gradient (5-30%) in 5 mM ammonium formate (pH 10). Fractions were collected at 1 min intervals, and pooled at various intervals to 12 fractions. Subsequently, the samples were dried and resuspended in 1% formic acid/5% ACN.

*Data-dependent acquisition (DDA) analysis and database searching*. The DDA analysis is used to generate a spectral library. DDA analysis was performed on an Orbitrap Fusion LUMOS Tribrid mass spectrometer (Thermo Fisher Scientific, Inc.) connected to an Easy-nLC 1200 via an Easy Spray (Thermo Fisher Scientific, Inc.). The peptide mixtures were loaded onto a self-packed analytical PicoFrit column with an integrated spray tip (75 $\mu$m x 40 cm length; New Objective) packed with ReproSil-Pur 120A C18-AQ (1.9 $\mu$m; Dr. Maisch GmbH) and separated within a 120 min linear gradient from 95% solvent A (0.1% formic acid/2% ACN/98% water) to 28% solvent B (0.1% formic acid/80% ACN) at a flow rate of 250 nl/min at 50˚C. Positive ion spray voltage was 1,900 V and the temperature of the Ion transfer tube was 275˚C. The mass spectrometer was operated in the positive-ion mode and employed in the data-dependent mode within the specialized cycle time (3S) to automatically switch between MS and tandem MS (MS/MS) with a maximum injection time of 500 msec. One full MS scan from 350-1,500 m/z was acquired at high resolution (R=120,000; defined at m/z=400); MS/MS scans were performed at a resolution of 30,000 with an isolation window of 4 Da and higher energy collisional dissociation (HCD) fragmentation, with collision energy of 30±5%. Dynamic exclusion was set to a time of 30 sec.

*Spectral library generation*. All the raw data, including depleted and undepleted samples of each fraction, were analyzed to generate the spectral library using the Pulsar search engine (only available in Spectronaut Pulsar; Biognosys AG). DDA raw data were searched against the human UniProt FASTA database (https://www.uniprot.org/proteomes/; 73,928 entries; downloaded on 1 April 2019) within the default parameters. In brief, the digestion enzyme allowed was specifically for trypsin enzyme with 2 missed specialized cleavages, and carbamidomethylation of cysteine was specified as the fixed modification, with oxidation of methionine as a variable modification. iRTs were calculated derived from median SiRTs across all DDA runs. Fragment ions for the targeted data analysis were selected from 300-1,800 m/z, the minimal relative intensity was set to >5%, and the fragment ion number was >3. The false discovery rate (FDR) was set to 1% for protein and peptide spectrum matches. Protein inference was performed using the ID Picker algorithm integrated within the Spectronaut software.

*Data-independent acquisition (DIA) sample MS*. To best resolve the DIA data based on the spectral library of the DDA data, DIA MS/MS acquisitions were performed with the same LC-MS systems and the same LC linear gradient method as for DDA. For the MS/MS acquisition, the DIA method involved setting 47 variable isolation windows according to the full width at half-maximum value, and the specific window lists were constructed based on the respective DDA data of the pooled serum or tears sample. The full scan was set at a resolution of 120,000 over an m/z range of 350-1,500, followed by DIA scans with resolution 30,000 [collision energy (CE), 30±5%; AGC target, 1e6; and maximal injection time, 54 msec].

*DIA data analysis*. DIA raw files were analyzed in Spectronaut X (Biognosys). The default settings were used for targeted analysis of DIA data in Spectronaut. Briefly, the retention time prediction type was set to dynamic iRT mode, and correction factor for window 1. Interference correction at the MS2 level was enabled. Systematic variance was normalized using the local normalization strategy. The FDR was estimated with the mProphet approach, and set to 1% at the peptide precursor level, and at 1% at protein level. The protein intensity was summed by the intensity of their respective peptides, which were calculated according to the peak areas of their respective fragment ions of MS2. All results were filtered using a Q-value cutoff of 0.01 (corresponding to an FDR of 1%).

*Bioinformatics analyses*. The output file from the Spectronaut software was used for further statistics and bioinformatics analyses. Normalization was performed on each sample according to the mean values. ANOVA (stats package included in R v.3.5.1) was used for the protein abundance calculation. Independent sample and paired-sample t tests were used between the healthy controls vs. patients with TAO and patients pre- and post-decompression, respectively. Differently expressed proteins (DEPs) were filtered if the fold change was >2.0, with $P<0.05$. Hierarchical cluster analysis is an algorithmic approach that enables discrete groups with varying degrees of (dis)similarity in a data set represented by a (dis)similarity matrix to be found. In the present study, this analysis was processed using a pheatmap package (version 1.0.12) at https://CRAN.R-project.org/package=pheatmap. Partial least squares discriminant analysis (PLS-DA) was used for multivariate data analysis (https://www.r-bloggers.com/classification-with-o-pls-da/). The volcano plot, which plots significance vs. fold-change on the $y$ and $x$ axes, respectively, is a type of scatterplot that is used to quickly identify changes in large data sets composed of replicate data. It is drawn by using a ggplot2 package (version 2.2.0 at http://ggplot2.org). Blast2GO version 5 (www.blast2go.com/) was used for functional annotation. The whole-protein sequence database was analyzed by BlastP (https://blast.ncbi.nlm.nih.gov/Blast.cgi) using whole database and mapped and annotated using the Gene Ontology (GO) database (http://geneontology.org/). Statistically altered functions of DEPs were calculated by Fisher's exact test in BLAST2GO. Pathway analysis was processed using Kyoto Encyclopedia of Genes and Genomes (KEGG) Orthology-Based Annotation System (KOBAS; http://kobas.cbi.pku.edu.cn/kobas3/?t=1). Clusters of Orthologous Groups (COG) and EuKaryotic Orthologous Groups (KOG) analysis was based on the phylogenetic classification of proteins encoded in complete genomes NCBI project (www.ncbi.nlm.nih.gov/COG/). Protein-protein interaction (PPI) networks were constructed using STRING v11 (www.string-db.org). Chord diagrams were mapped using the circlize package (version 0.4.6) developed by Zuguang Gu in R (http://www.r-graph-gallery.com/123-circular-plot-circlize-package-2/).

*g:Profiler analysis*. GO analysis [molecular function (MF), cellular component (CC) and biological process (BP)] was performed using g:Profiler (https://biit.cs.ut.ee/gprofiler/). The parameters for the enrichment analysis were as follows: A specific organism was chosen [*Homo* (*H.*) *sapiens*]. The version of g:Profiler was e95_eg42_p13_f6e58b9 (database updated on 26 May 2019). Biological pathways were enriched in the GO, KEGG and Reactome (REAC) pathway databases. The protein databases were used the Human Protein Atlas (http://www.proteinatlas.org/) and CORUM databases (http://mips.helmholtz-muenchen.de/corum/). The statistical domain scope was used only for annotated genes. The significance threshold was the g:SCS threshold. The g:SCS method is used for computing multiple testing corrections for P-values gained from GO and pathway enrichment analysis, and the user threshold was set to 0.05.

*NetworkAnalyst analysis*. The website for NetworkAnalyst analysis was upgraded and maintained until May 8, 2019 by the Xia Lab (https://www.networkanalyst.ca/NetworkAnalyst/faces/home.xhtml). The parameters for the enrichment analysis were as follows. The specific organism chosen was *H. sapiens*. The MEx Interactome database (http://www.innatedb.com) was used to analyze the PPIs. The parameters were referred to literature-curated comprehensive data from InnateDB (26). Comprehensive experimentally validated microRNA (miRNA/miR)-gene interaction data were collected from miRTarBase (http://mirtarbase.cuhk.edu.cn/php/download.php), whereas the ENCODE database (http://cistrome.org/BETA/) was used to explore transcription factor (TF)-gene interactions. TF and gene target data were derived from the ENCODE ChIP-seq data. Literature-curated regulatory TF-miRNA co-regulatory interaction network information was collected from the RegNetwork repository (http://www.regnetworkweb.org/).

*REAC enrichment analysis*. The enrichment analysis was performed against REAC version 66 (https://reactome.org/PathwayBrowser) on 25 May 2019 using UniProt identifiers for the mapping. REAC analysis was performed as described previously (27). The parameters for the enrichment analysis were as follows: A specific organism was chosen (*H. sapiens*), and an overrepresentation analysis method was used for the enrichment analysis. This test produces a probability score, which is corrected for the FDR using the Benjamini-Hochberg (BH) method (28).

*Statistics*. The statistical software package SPSS 19.0 (IBM Corp.) was used for statistical analysis. The measured values are presented as the mean ± SD. For bioinformatics analyses, FDR was set to 1% for protein and peptide spectrum matches. The adjusted P-value (adjP) method used was the BH method, and adjP values were transformed to negative log10 [-log10(adjP)].

## Results

*Orbital decompression ameliorates exophthalmos in inactive TAO patients*. Six patients with inactive TAO with only one exophthalmia were chosen for this investigation. The CASs and levels of thyroid hormone function-associated hormones in these cases were found to be relatively normal (data not shown). The OSDI score of the inactive TAO cases was significantly increased compared with that of the healthy control group (18.0±1.7 for the patients with TAO before orbital decompression surgery compared with 6.2±2.3 for the control subjects; P<0.01; Table I). After orbital decompression surgery, the OSDI score of the patients with TAO measured 15.6±3.0, reflecting a small (non-significant) decrease in OSDI score of 2.4 compared with before their surgery. The palpebral fissure was subsequently determined using a 3D reconstruction of orbital CT with Mimics software. The palpebral fissure height and area of the exophthalmia were significantly increased compared with their normal eyeballs in these patients (Table II). Orbital decompression was performed to ameliorate the disfiguring exophthalmos. The exophthalmia was reversed, and the values were within the normal ranges after 1 month of decompression. The degree of exophthalmos of these patients was reduced by >3 mm. In addition, the palpebral fissure height was also reduced by 1.7 mm. Moreover, the clinical symptoms of exophthalmia, such as conjunctival hyperemia, edema and dry eye, were markedly improved.

Table I. OSDI scores of patients with TAO and healthy controls.

| Group | OSDI score |
|---|---|
| CTL | 6.2±2.3 |
| TAO | |
| BS | 18.0±1.7[a] |
| AS | 15.6±3.0 |

[a]P<0.01 vs. CTL. OSDI, ocular surface disease index; TAO, thyroid-associated ophthalmopathy; BS, before orbital decompression surgery; AS, after orbital decompression surgery; CTL, healthy control. An independent t test was used between the CTL and TAO group, while a paired-sample t test was used between the patients pre- and post-decompression.

*Tear proteomics changes among healthy case subjects, and preoperative and postoperative patients with TAO*. LC-MS/MS analysis was performed to identify proteins following tear collection and processing, as described in the Materials and methods section. PLS-DA of the proteomics results indicated that differences in the protein composition of tears from patients within the same group was not notable, whereas difference in tears from patients in the different groups were significant (Fig. 1A). A total of 669 proteins were identified by LC-MS/MS (Fig. 1E; for more information, refer to Table SI). Among the 669 proteins, the expression levels of 83 of them were significantly changed (Table SI). Among the 83 DEPs, 51, 81 and 47 proteins were identified in the healthy control group, the preoperative and postoperative stages of the patients with inactive TAO, respectively (Fig. 1B). Venn and chord diagrams of these DEPs (Fig. 1B and C, respectively) show the distribution of these proteins. A heatmap

Table II. Palpebral fissure measurements of patients with thyroid-associated ophthalmopathy.

| | | Exophthalmos | | |
|---|---|---|---|---|
| Measurement | NCE | BS | AS | Change |
| Area, $mm^2$ | 143.12±30.29 | 200.70±29.30[b] | 142.58±27.20[d] | -58.12 |
| Height, mm | 9.13±1.15 | 10.89±1.29[a] | 9.18±1.21[c] | -1.71 |
| Breadth, mm | 27.80±1.46 | 27.84±1.47 | 27.80±1.49 | -0.04 |

[a]P<0.05, [b]P<0.01 vs. NCE; [c]P<0.05, [d]P<0.01 vs. BS. NCE, healthy eye of patients with TAO with only one exophthalmia; BS, before orbital decompression surgery; AS, after orbital decompression surgery. Changes represents alterations from preoperative to postoperative TAO.

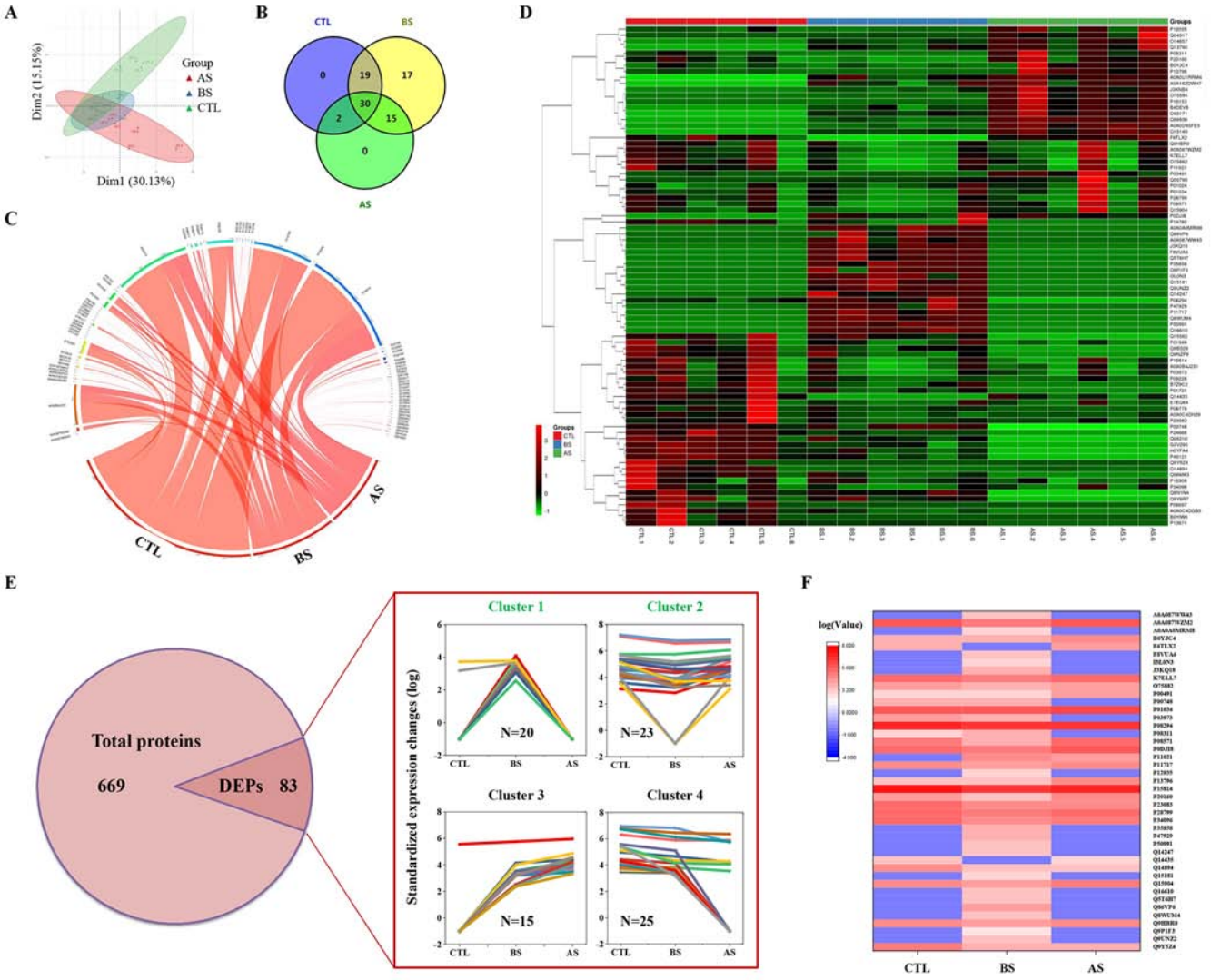


Figure 1. Tear proteomics of the patients with inactive TAO before and after orbital decompression as determined via liquid chromatography with tandem mass spectrometry. (A) Partial least squares-discriminant analysis of proteomics data. (B) Venn diagram and (C) chord diagram of the DEPs. (D) Heatmap of the DEPs. (E) Numbers of proteins, and relative protein expression levels of the DEPs. (F) Heatmap of candidate DEPs in (clusters 1 and 2). CTL, healthy control; BS, before orbital decompression surgery; AS, after orbital decompression surgery; DEP, differentially expressed protein; TAO, thyroid-associated ophthalmopathy.

of the DEPs was constructed to show the clustering of the associations of these proteins (Fig. 1D). Four clusters of DEPs were identified within the DEPs by comparing their expression levels (Fig. 1E). Among them, clusters 1 and 2 were selected and mapped within a heatmap, since their expression was consistent with the prognosis of decompression (Fig. 1F). A total of 43 DEPs were found among these two clusters.

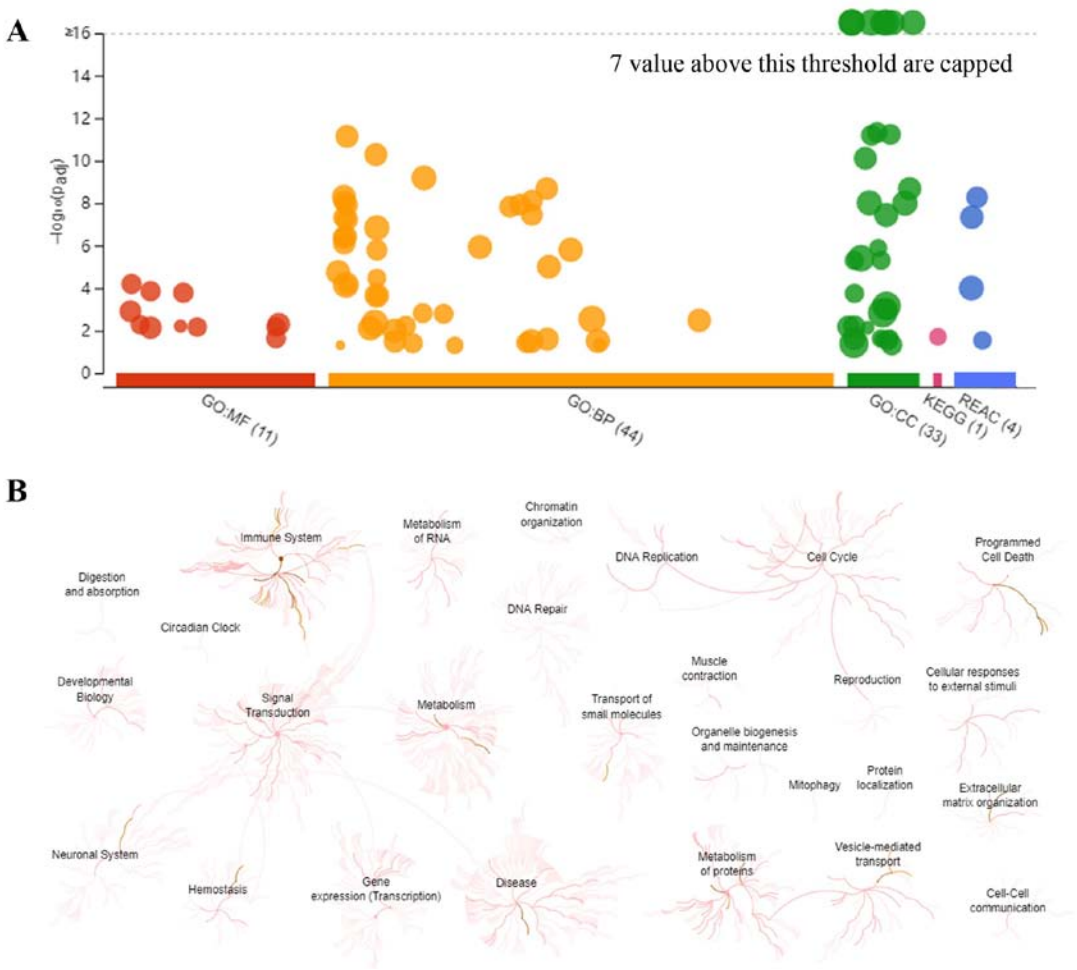


Figure 2. Overall results of bioinformatics analyses using g:Profiler and REAC. (A) Significantly enriched terms in the GO, KEGG and REAC databases (the terms for GO:MF, GO:BP, GO:CC, KEGG and REAC are color-coded red, orange, green, magenta and blue, respectively). (B) Enrichment pathways and their interactions enriched by REAC are shown. GO, Gene Ontology; KEGG, Kyoto Encyclopedia of Genes and Genomes; MF, molecular function; BP biological process; CC, cellular component; REAC, reactome pathway.

*Results of the enrichment analyses performed with g:Profiler and REAC*. To visually reveal the enrichment pathways of the DEPs, g:Profiler and REAC analyses were performed. A large number of pathways were enriched according to g:Profiler analysis of the GO, KEGG, and REAC databases (Fig. 2A). Additionally, extensive interactions existed between these enrichment pathways (Fig. 2B). For example, the 'signal transduction' pathway interacted with 'immune system', 'metabolism', 'neuronal system', 'hemostasis' and 'gene expression'.

To explore the categories of these enrichment pathways, 45 REAC-enriched pathways were further classified and analyzed (Fig. 3A). Pathways were predominantly associated with 'immune system', 'metabolism', 'programmed cell death' and 'vesicle-mediated transport', with up to 79% of pathways enriched with DEPs involved in these processes (Fig. 3B). In addition, other pathways were involved in 'extracellular matrix (ECM) organization', 'hemostasis' and the 'neuronal system' (Fig. 3B). Additionally, the interactions among these enriched pathways were analyzed by NetworkAnalyst. A large number of interactions were found among these pathways (Fig. 3C). For example, 'regulation of insulin-like growth factor (IGF) transport and uptake by IGF-binding proteins (IGFBPs)' interacted with 'metabolism of proteins', 'activation of matrix metalloproteinases', 'activation of chaperones' and other processes.

*Results of the GO enrichment analysis*. GO enrichment analysis was further employed to explore the enriched BP, MF and CC terms. A total of 44 BP, 11 MF and 33 CC terms were significantly enriched according to the g:Profiler analysis with an adj $P<0.05$, respectively. For the BP terms, 'immune response', 'defense response', were among the major terms, according to the percentages of proteins identified (Fig. 4A and B). For the MF terms, 'hydrolase activity', 'peptidase activity' and 'endopeptidase activity' were the top terms, according to the percentages of proteins identified (Fig. 4A and C). Finally, 'extracellular region part', 'organelle', 'vesicle' and 'extracellular exosome' were the top CC terms (Fig. 4A and D).

The interactions of these GO terms were further analyzed using NetworkAnalyst. A large number of interactions were enriched according to the GO terms (Fig. 4E-G). For instance, 'inflammatory response' interacted with the 'defense response', 'response to wounding' and 'immune response' in the BP term category (Fig. 4E). 'Glycosaminoglycan binding', 'endopeptidase activity', 'serine hydrolase activity',

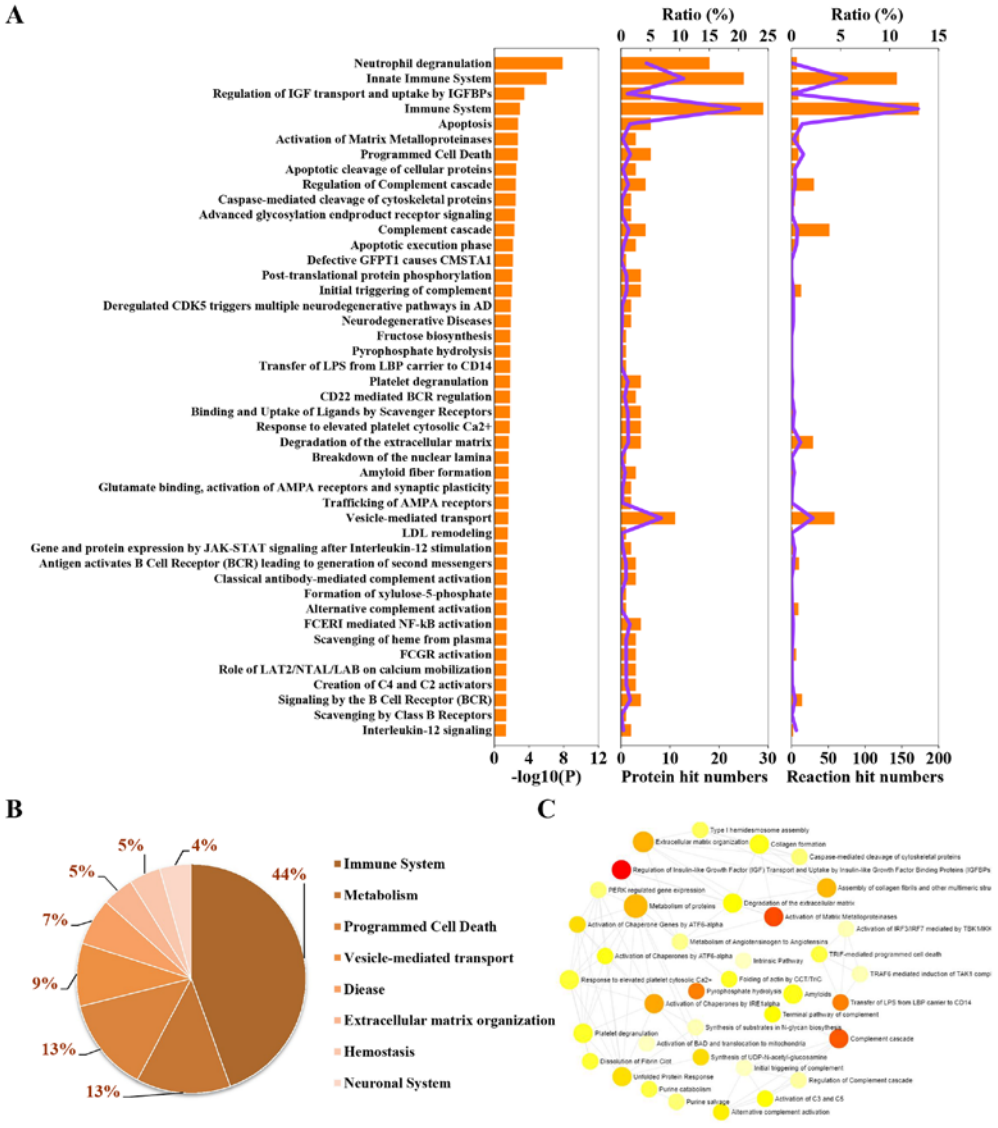


Figure 3. Classification statistics of significantly enriched Reactome pathways. (A) Left, enrichment pathways in the order of-log(adjP); middle, numbers and ratios of DEPs involved in enrichment pathways are shown as the combined columns and line chart; right, numbers and ratios of reactions are shown as the combined column and line chart. (B) Statistical analysis of the results of the classification shown in (A). (C) Interactions among the significantly changed pathways according to NetworkAnalyst. The size of the icon indicates gene hit numbers in pathways. The bigger the size, the greater the gene hit number. The color indicates the-log10 (P-value). The darker the color, the larger the-log10 (P-value).

'serine-type peptidase activity' and 'serine-type endopeptidase activity' interacted with each other in the MF term category (Fig. 4F). Finally, 'vesicle', 'lysosome', 'vacuole', 'extracellular region' and other CC terms interacted (Fig. 4G).

*Results of the KEGG enrichment analysis*. The enriched signaling pathways and their interactions according to KEGG were subsequently analyzed using KOBAS and NetworkAnalyst. Ten significant signaling pathways were enriched according to KOBAS (Fig. 5A). Among them, pathways involved in the 'complement and coagulation cascades', 'tuberculosis', 'salivary secretion', 'systemic lupus erythematosus', 'lysosome' and 'protein processing in endoplasmic reticulum' were abundant, and their ratios were as high as 71% (Fig. 5B). Additionally, 'complement and coagulation cascades', 'lysosome' and 'phagosome' were pathway terms that interacted with various diseases (Fig. 5C).

*Results of the KOG enrichment analysis*. KOG enrichment analysis was subsequently performed using KOBAS. A total of 20 function classes were enriched (Fig. 6A). Among them, 'protein synthesis, transport and metabolism', 'signal transduction mechanisms', 'cytoskeleton', 'general function prediction', 'energy production and conversion', 'immune system', 'extracellular structures' and 'transport and metabolism' were most prevalent, and the sum of their ratios reached as high as 80.9% (Fig. 6B).

*PPIs and gene regulatory network results of DEPs*. In order to explore the PPIs and gene regulatory networks, NetworkAnalyst and STRING analyses were performed. A large number of interactions were found to be enriched. The proteins CAND1, HSPA5, YWHAH, PDCD6IP, CTTN and CCT4 frequently interacted with other proteins via PPIs (Fig. 7A). In the TF-gene interactions, TFs such as MAZ, SMAD5, ZNF580 and TFDP1 regulated the

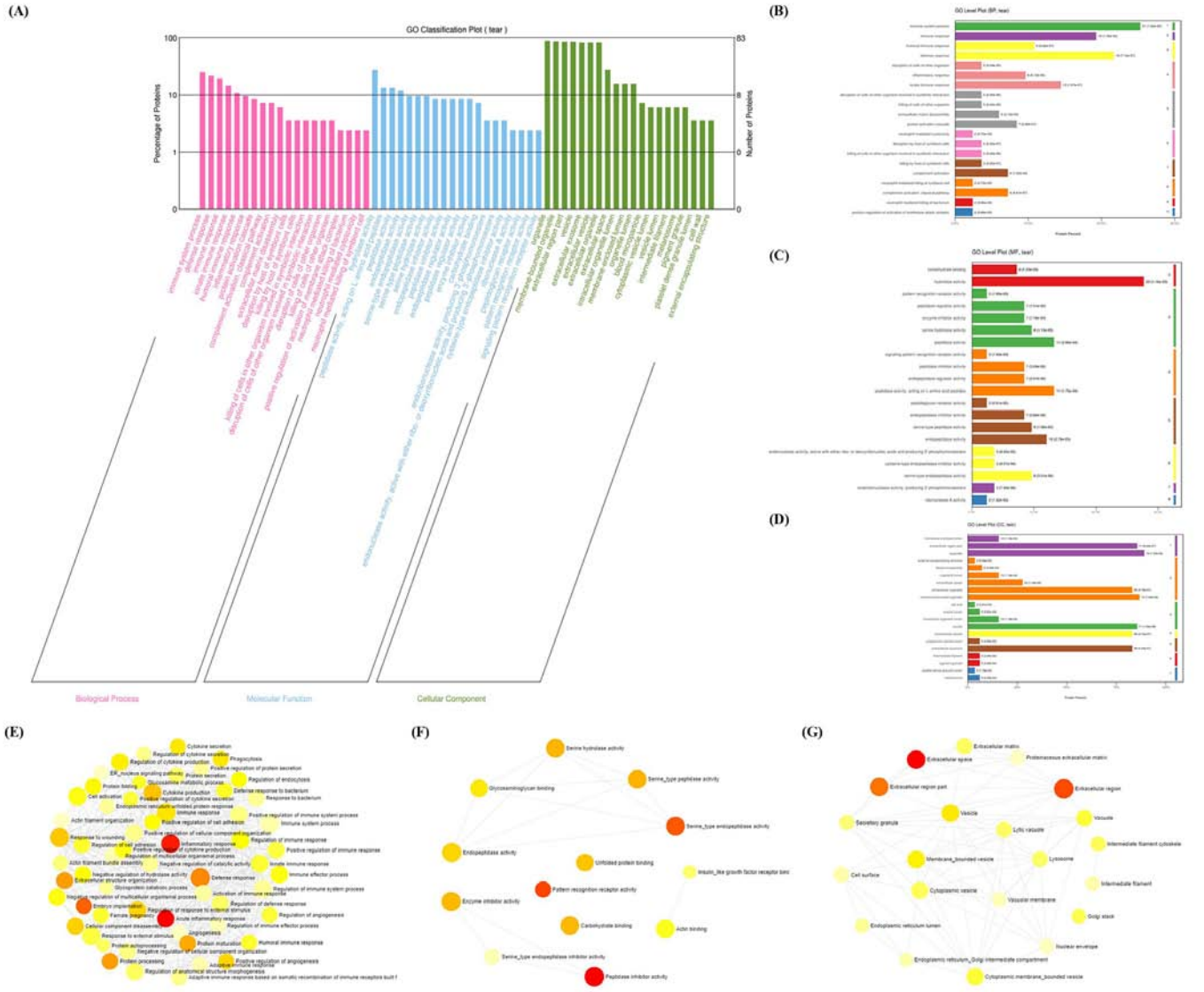


Figure 4. GO enrichment analysis. (A) Enriched BP, MF and CC terms according to Blast2GO. (B) BP, (C) MF and (D) CC level plots were constructed according to Blast2GO. Interactions of GO (E) BP, (F) MF and (G) CC terms by NetworkAnalyst. GO, Gene Ontology; MF, molecular function; BP biological process; CC, cellular component. The size of the icon indicates gene hit numbers in pathways. The bigger the size, the greater the gene hit number. The color indicates the-log10 (P-value). The darker the color, the larger the-log10 (P-value).

expression of genes such as PLEC, VAT1, C3, CAPG, CST3, IGF2R, PNP, GRN, PDCD6IP, CAND1, ATP6AP1 (Fig. 7B). Furthermore, in the TF-microRNA co-regulatory interactions, miRNAs such as hsa-miR-30a and hsa-miR-506 co-regulated TFs such as EGR1, GABPA, FOS, MAX and JUN, thus also regulating the expression of YWHAH, VAT1, TGFBI, PLEC, HSPA5, CAND1, PDCD6IP and MMP9 (Fig. 7C). PPIs were then further analyzed using STRING, and it was found that CTSG, C3, AZU1, VAT1, PGLYRP1, GRN, RNASE2, MMP9, SLPI and ERP44 were the core proteins (Fig. 7D).

## Discussion

In the present study, orbital decompression was shown to significantly ameliorate disfiguring exophthalmos in patients with inactive TAO. Among 669 proteins identified by proteomics, the levels of 83 proteins were changed significantly before and after orbital decompression surgery, and between patients and healthy subject groups. Bioinformatics analyses indicated that pathways involved in 'immune system', 'metabolism', 'programmed cell death', 'vesicle-mediated transport', 'neuronal system' and 'ECM organization signaling' processes may fulfill important roles in orbital decompression for patients with inactive TAO. Examples of involved processes include 'neutrophil degranulation', 'glutamate binding', 'activation of α-amino-3-hydroxy-5-met hyl-4-isoxazolepropionic acid (AMPA) receptors and synaptic plasticity', 'immune system' and 'regulation of IGF transport and uptake by IGFBPs'. A large number of interactions that existed in TF-miRNA co-regulatory interactions were identified. These results provided a preliminary understanding of the mechanisms involved in orbital decompression for disfiguring exophthalmos in patients with inactive TAO.

Chronic inflammation has a key role in high blood pressure (29). In patients with TAO, long-term intraocular pressure increase results from episcleral venous pressure elevation (30).

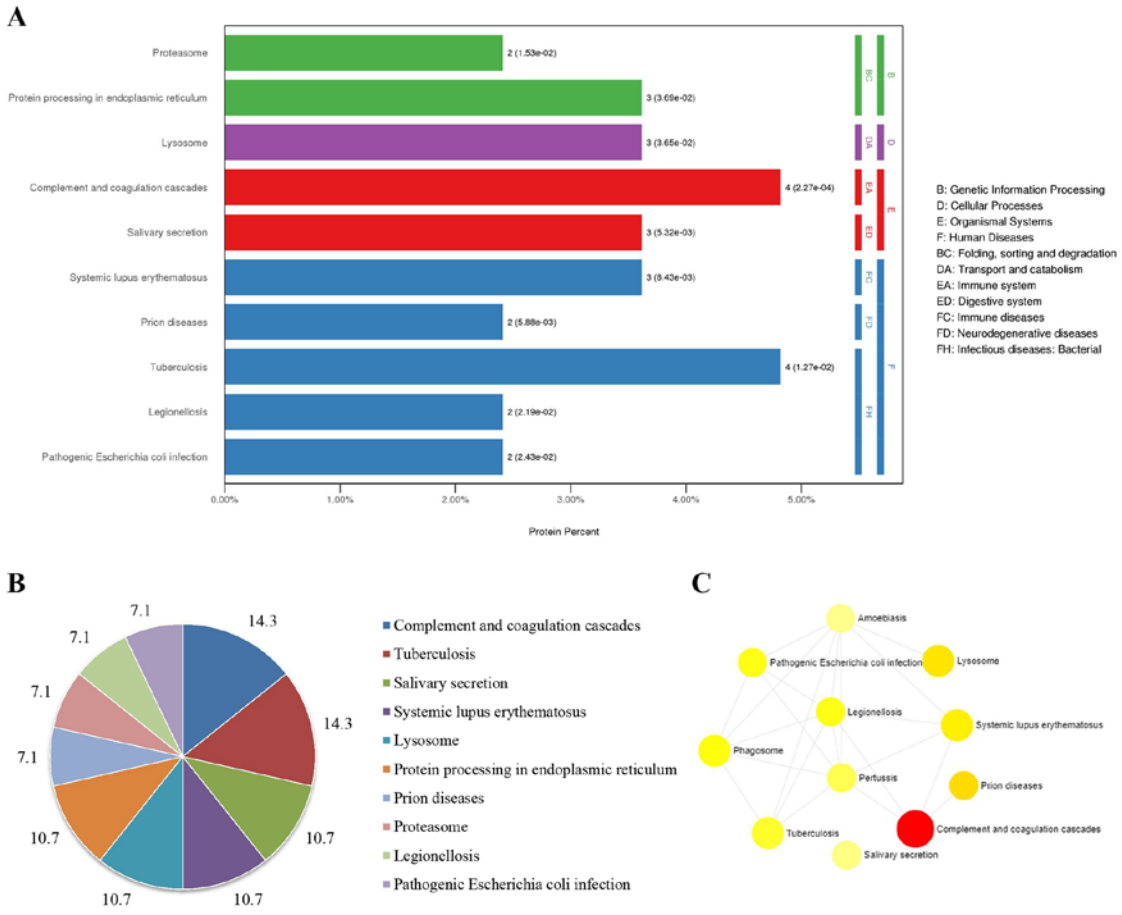


Figure 5. KEGG enriched pathways and their interactions using KOBAS and NetworkAnalyst. (A) Enriched pathways by KOBAS. (B) Pie chart of the percentages of the enriched pathways identified by KOBAS. (C) Interactions of KEGG pathways. KEGG, Kyoto Encyclopedia of Genes and Genomes. The size of the icon indicates gene hit numbers in pathways. The bigger the size, the greater the gene hit number. The color indicates the-log10 (P-value). The darker the color, the larger the-log10 (P-value).

Inflammatory markers, such as high-sensitivity C-reactive protein, IL-6 and amyloid A, are associated with a larger retinal venular diameter (31). These findings suggest that the persistent elevation of intraocular pressure and inflammation may interact with each other, leading to the deterioration of exophthalmos in patients with TAO. Additionally, an immunogenic mechanism of pathogenesis has been proposed, and immunosuppressive therapy has been shown to decrease immunological processes in TAO (32). In the present study, it was shown that immune system pathways, such as 'neutrophil degranulation', 'innate immune system' and 'regulation of complement cascade', were enriched by REAC analysis. Among these pathways, A0A087WZM2, P00491, P01034, P03973, P08311, P08571, P20160, P23083 and Q9Y5Z4 proteins were decreased, whereas P0DJI8, P11717 and P28799 were increased in the TAO group compared with the healthy group (Table SI). Orbital decompression led to a significant recovery of these abnormal DEPs. Taken together, these data indicated that a decrease in the elevated eyeball pressure by decompression may ameliorate immune dysfunction in patients with TAO.

In addition to inflammation, orbital fibroblasts have been proposed to be involved in the pathology of TAO (33). A previous study demonstrated that orbital fibroblasts separated from patients with TAO produce significantly higher levels of IL-6, IL-8, and monocyte chemoattractant protein-1 through CD40 ligation than orbital fibroblasts from control case subjects (34). In addition, CD40/CD154 and IL-1 promote IL-6 and IL-8 production in orbital fibroblasts (33,34). Elevated local levels of IL-6 in the orbit may enhance lymphocyte activation or recruitment (35). In addition, the Janus kinase (JAK)-STAT signaling pathway was activated via the production of CD40 in orbital fibroblasts induced by interferon-γ (33). In the present study, gene and protein expression by JAK-STAT signaling following IL-12 stimulation mediated by A0A0D9SFE5 and P13796 was enriched (Table SI). This suggested that the JAK-STAT pathway has a significant role in the production of proinflammatory cytokines by orbital fibroblasts in patients with TAO. Additionally, rollback of exophthalmos through orbital decompression may be mediated via JAK-STAT signaling.

The disordered accumulation of hyaluronan, a non-sulfated glycosaminoglycan ECM component, is associated with TAO (36). Hyaluronan accumulation is attributed to perimysial orbital fibroblasts (37). Following activation with proinflammatory cytokines, orbital fibroblasts were able to enhance the production of hyaluronan synthesis. Therefore, the accumulation of hyaluronan was proposed as a hallmark

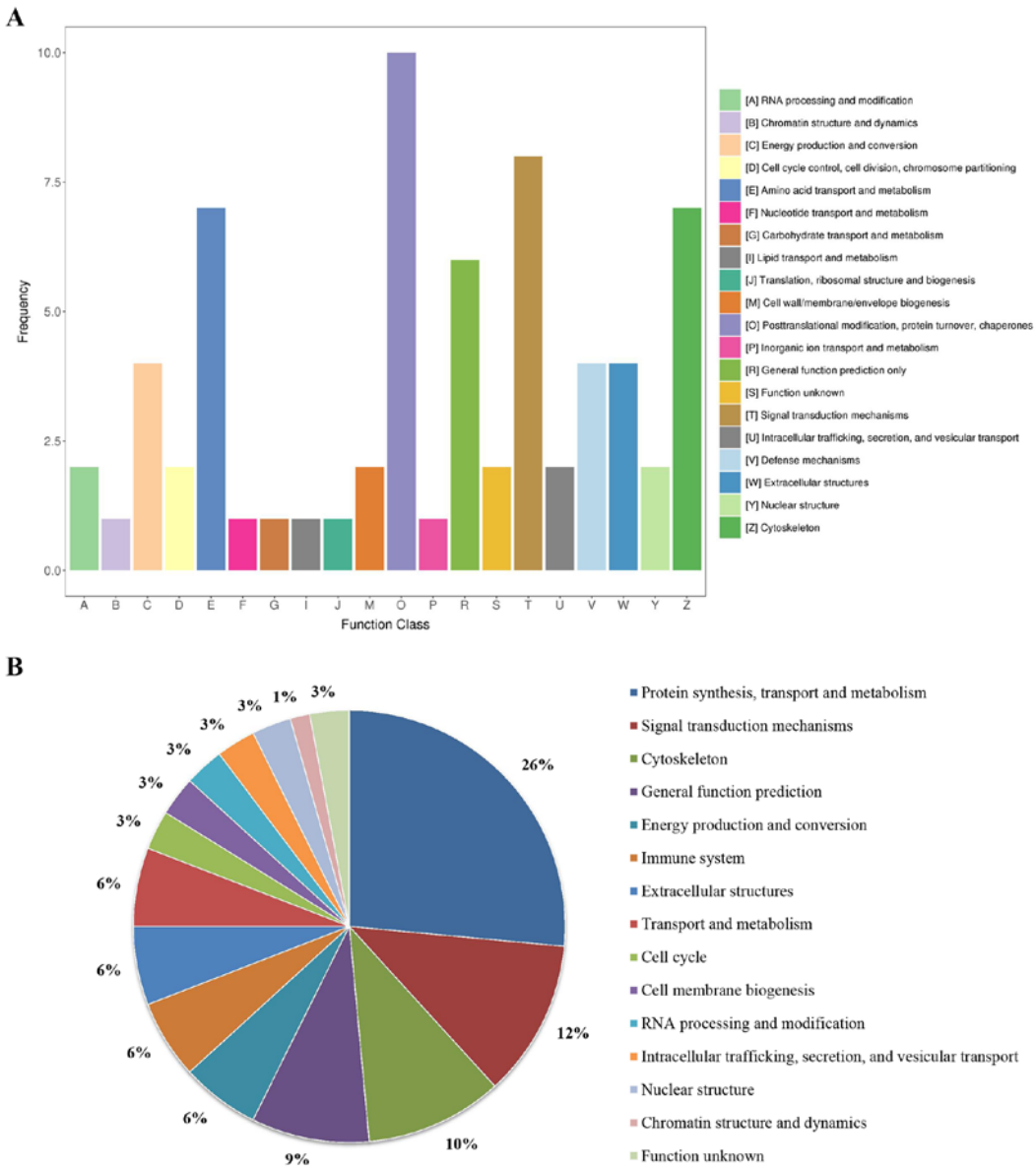


Figure 6. Results of the KOG enrichment analysis by KOBAS. (A) KOG pathways. (B) Pie chart of percentages of these enriched pathways. KOG, EuKaryotic Orthologous Groups.

feature of tissue remodeling in TAO (38). It appears that the disordered accumulation of ECM components may be conducive to aggravating the elevated eyeball pressure, resulting in an imbalance between the immune system and local pressure in orbita. In the present study, it was shown that decompression activated the degradation of ECM signaling mediated by A0A0C4DGB5, E7EQ64, P14780 and P08311. In addition, matrix metalloproteinases were also activated by decompression (Table SI). These data indicated that the degradation of ECM components through decompression exerts important roles in ameliorating the elevation of ocular pressure.

Scavenger receptors represent an important part of the innate immune defense by acting as pattern-recognition receptors, in particular against bacterial pathogens (39). Additionally, to reduce the discomfort caused by exophthalmos in patients with TAO, such as itching, swelling, pain and a burning sensation, patients may uncontrollably increase the chance of touching, wiping or squeezing the eyeball, especially in the absence of consciousness, which undoubtedly increases the probability of eye infection (40). Decompression may relieve some discomfort by directly reducing eye pressure, and ultimately, may indirectly reduce the potential risk of infection. In the present study, 'binding and uptake of ligands by scavenger receptors', one form of vesicle-mediated transport signaling, was enriched according to the bioinformatics analyses. The enriched results suggested that binding and uptake of ligands by scavenger receptors may have a key role in orbital decompression for TAO.

AMPA receptors, key regulators of neurotransmitter receptors and postsynaptic signal transmission under conditions of basal neuronal activity, have a major role in the strength of the synaptic response (41). Intracerebral injection of AMPA causes a significant increase in damage to axons and myelin (42). Additionally, AMPA receptor antagonists decrease neuronal

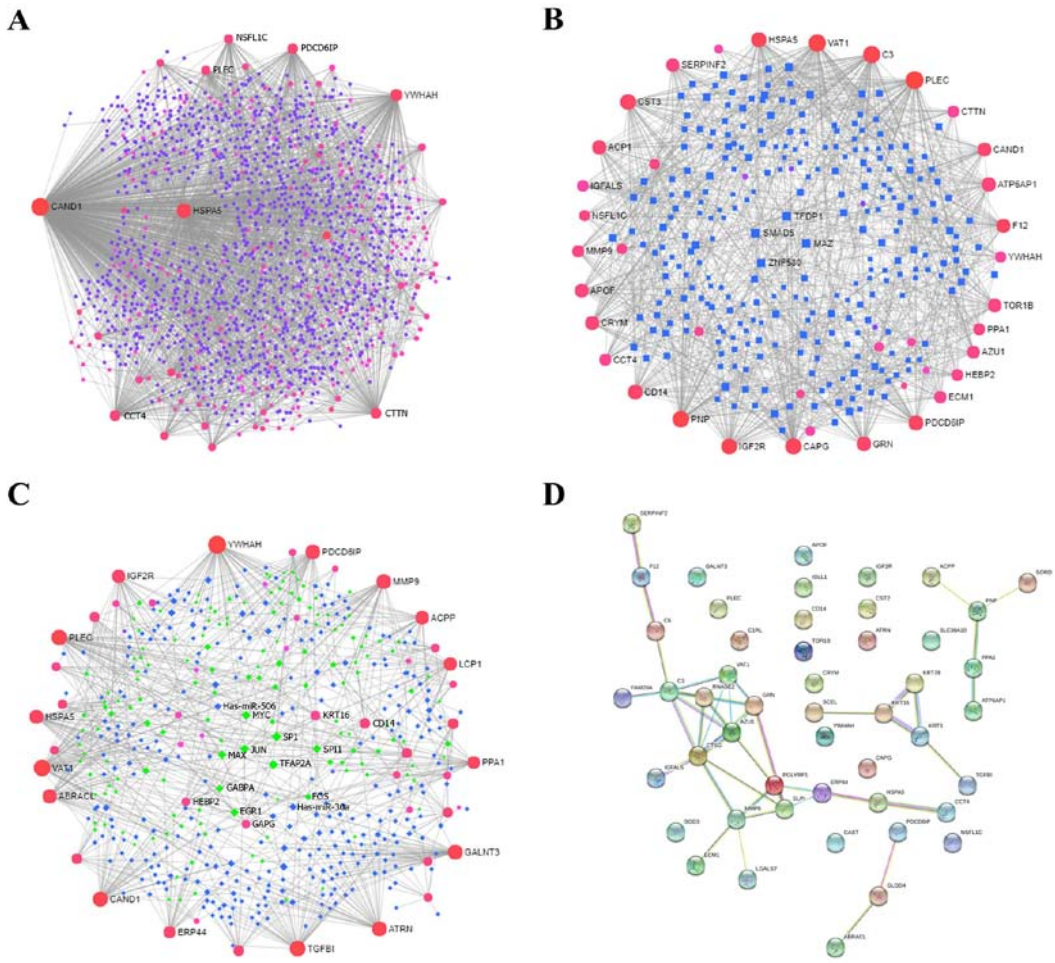


Figure 7. PPIs and gene regulatory networks analysis of DEPs. (A) PPIs, (B) TF-gene interactions and (C) TF-miRNA coregulatory interactions were assessed using NetworkAnalyst. The size of the icon indicates gene hit numbers in pathways. The bigger the size, the greater the gene hit number. The color indicates the-log10 (P-value). The darker the color, the larger the-log10 (P-value). (D) PPIs according to STRING analysis. PPI, protein-protein interaction; DEP, differentially expressed protein; TF, transcription factor.

damage (43). Recently, our research group reported that the central corneal sub-basal nerve plexus of patients with TAO was significantly decreased compared with those of control subjects, suggesting that nerve degeneration is associated with the disease (44). In the present study, trafficking of AMPA receptor signaling was enriched in orbital decompression. Although the mechanisms of central corneal sub-basal nerve plexus reduction have yet to be fully elucidated, the enriched results of the present study indicated that AMPA receptor signaling may be involved in orbital decompression for TAO.

Apoptosis, a form of programmed cell death, is crucial during embryonic development and is equally important for the maintenance of normal cellular homeostasis in adult organs. Fas-mediated apoptosis may occur in extraocular muscle tissue from patients with TAO, and may be involved in the late stage of TAO (45). In addition, inducing lacrimal gland inflammation led to increased acinar cell apoptosis (46). Additionally, apoptosis has been proposed as a possible mechanism responsible for the impairment of lacrimal gland secretory function associated with Sjogren syndrome (47,48). The results of the present study demonstrated that apoptosis, which is increased according to the bioinformatics analyses, may have a key role in orbital decompression for TAO. Although the effect of apoptosis on TAO progression requires further clarification, orbital decompression may regulate apoptosis mediated by Q15149, A0A0D9SFE5, P08571, G3V295, B0YJC4 and Q04917.

The abnormal accumulation of amyloid, typically extracellular deposits of fibrillar proteins, is associated with nerve damage in neurodegenerative diseases. Enrichment analyses revealed that amyloid fiber formation, a signaling pathway associated with the metabolism of proteins, is involved in orbital decompression of TAO (Table SI). Additionally, regulation of IGF transport and uptake by IGFBPs is also involved in orbital decompression for TAO. A previous study confirmed that teprotumumab, a monoclonal antibody against IGF-I receptor, significantly reduced proptosis in TAO patients (49). These findings indicated that signaling pathways associated with the metabolism of proteins, such as IGF transport and uptake by IGFBPs and amyloid fiber formation, may have significant roles in orbital decompression for exophthalmos in patients with TAO.

In addition to inflammation, the pathogenesis of TAO involves apoptosis, ECM component accumulation, neurodegeneration, orbital fibroblasts and increased fat volume (33,38,44,45). The potentially complex interaction among mononuclear cells, fat cells and orbital fibroblasts may

underlie the unusual tissue reactivity and remodeling that occurs in patients with TAO. The tear proteomics and bioinformatics analysis results of the present study suggested that decompression-mediated direct reduction of eyeball pressure appears to relieve or interrupt the vicious cycle of pressure and inflammation, and then regulate subsequent metabolism, vesicle-mediated transport, nervous system abnormalities, and ultimately reduce exophthalmos in patients with inactive TAO.

There are certain limitations to the present study. Although FDR <0.01, and not FDR <0.05, was selected as the threshold in the present study, there is still close to 1% false-positive rate. More direct evidence is therefore required to substantiate the reported results. Due to technical problems that exist with western blotting detection of lacrimal proteins, validation experiments can only be performed when these issues have been resolved. Parallel reaction monitoring or a multiple reaction monitoring mass spectrometry (MRM-MS) based targeted proteomic strategy may also be used for validation in the future. Additionally, an examination of the changes of tear proteomics between the inactive and the active stage in the same group of patients recruited for the present study would provide more information regarding the underlying mechanisms of TAO. Such experiments are currently under way to reveal the pathogenesis of TAO. Furthermore, orbital decompression is suitable for TAO cases in the inactive stage, but not in the active stage. Therefore, inactive TAO patients were selected for the present study. As the eyeball parameters of different subjects are quite different, inactive TAO patients with unilateral exophthalmos were selected in the present study. It is relatively difficult to obtain larger numbers of inactive TAO cases, even in Chinese hospitals. Therefore, only six patients were included in the present study.

In the present study, it was shown that the exophthalmia were restored to normal after 1 month of orbital decompression in patients with inactive TAO. A total of 83 proteins differed significantly among the preoperative and postoperative stages of inactive TAO, and between patients and healthy control subjects. Bioinformatics analyses revealed that immune system, metabolism, programmed cell death, vesicle-mediated transport, neuronal system, and ECM organization signaling pathways may have significant roles in orbital decompression for patients with inactive TAO. Taken together, the results of these proteomics and bioinformatics analyses have provided a preliminary understanding of the mechanisms underlying orbital decompression for disfiguring exophthalmos in patients with inactive TAO.

**Acknowledgements**

Not applicable.

**Funding**

The present study was supported by the National Natural Science Foundation of China (grant no. 81770959) and Shanghai Municipal Commission of Health and Family Planning (grant no. 201640215).

**Availability of data and material**

The datasets used and/or analyzed during the present study are available from the corresponding author on reasonable request.

**Authors' contributions**

AR made substantial contributions to conception and design. LJ acquired, analyzed and interpreted the data. RW, JD, HD and WW acquired the data.. LJ, HD and WW were involved in drafting and revising the manuscript. All authors read and approved the final manuscript.

**Ethics approval and consent to participate**

All protocols were approved by the Ethics Committee of Zhabei District Central hospital in accordance with the ethical standards stated in the Declaration of Helsinki. All patients provided written informed consent.

**Patient consent for publication**

Not applicable.

**Competing interests**

The authors declare that they have no competing interests.

**References**

1. Nishida Y, Tian S, Isberg B, Hayashi O, Tallstedt L and Lennerstrand G: Significance of orbital fatty tissue for exophthalmos in thyroid-associated ophthalmopathy. Graefes Arch Clin Exp Ophthalmol 240: 515-520, 2002.
2. Higashiyama T, Nishida Y and Ohji M: Changes of orbital tissue volumes and proptosis in patients with thyroid extraocular muscle swelling after methylprednisolone pulse therapy. Jpn J Ophthalmol 59: 430-435, 2015.
3. Ohtsuka K, Sato A, Kawaguchi S, Hashimoto M and Suzuki Y: Effect of high-dose intravenous steroid pulse therapy followed by 3-month oral steroid therapy for Graves' ophthalmopathy. Jpn J Ophthalmol 46: 563-567, 2002.
4. Prat MC, Braunstein AL, Dagi Glass LR and Kazim M: Orbital fat decompression for thyroid eye disease: Retrospective case review and criteria for optimal case selection. Ophthalmic Plast Reconstr Surg 31: 215-218, 2015.
5. Krönlein RU: Zur Pathologie und operativen behandlung der dermoidcysten der Orbita. Beitr Klin Chir 4: 149-163, 1889.
6. Zhang-Nunes SX, Dang S, Garneau HC, Garneau HC, Hwang C, Isaacs D, Chang SH and Goldberg R: Characterization and outcomes of repeat orbital decompression for thyroid-associated orbitopathy. Orbit 34: 57-65, 2015.
7. Bahn RS: Is orbital decompression a safe and effective treatment for Graves' orbitopathy? Nat Clin Pract Endocrinol Metab 3: 796-797, 2007.
8. Boboridis KG, Uddin J, Mikropoulos DG, Bunce C, Mangouritsas G, Voudouragkaki IC and Konstas AG: Critical appraisal on orbital decompression for thyroid eye disease: A systematic review and literature search. Adv Ther 32: 595-611, 2015.
9. Bahn RS and Heufelder AE: Pathogenesis of Graves' ophthalmopathy. N Engl J Med 329: 1468-1475, 1993.
10. Lim SL, Lim AK, Mumtaz M, Hussein E, Wan Bebakar WM and Khir AS: Prevalence, risk factors, and clinical features of thyroid-associated ophthalmopathy in multiethnic Malaysian patients with Graves' disease. Thyroid 18: 1297-1301, 2008.
11. Herbaut A, Liang H, Denoyer A, Baudouin C and Labbé A: Tear film analysis and evaluation of optical quality: A review of the literature (French translation of the article). J Fr Ophtalmol 42: 226-243, 2019 (In French).
12. Zhou L and Beuerman RW: The power of tears: How tear proteomics research could revolutionize the clinic. Expert Rev Proteomics 14: 189-191, 2017.
13. Janssen PT and van Bijsterveld OP: Origin and biosynthesis of human tear fluid proteins. Invest Ophthalmol Vis 24: 623-630, 1983.

14. Tsai PS, Evans JE, Green KM, Sullivan RM, Schaumberg DA, Richards SM, Dana MR and Sullivan DA: Proteomic analysis of human meibomian gland secretions. Br J Ophthalmol 90: 372-377, 2006.
15. Ji YW, Lee JL, Kang HG, Gu N, Byun H, Yeo A, Noh H, Kim S, Choi EY, Song JS and Lee HK: Corneal lymphangiogenesis facilitates ocular surface inflammation and cell trafficking in dry eye disease. Ocul Surf 16: 306-313, 2018.
16. Kishazi E, Dor M, Eperon S, Oberic A, Hamedani M and Turck N: Thyroid-associated orbitopathy and tears: A proteomics study. J Proteomics 170: 110-116, 2018.
17. Aass C, Norheim I, Eriksen EF, Børnick EC, Thorsby PM and Pepaj M: Comparative proteomic analysis of tear fluid in Graves' disease with and without orbitopathy. Clin Endocrinol (Oxf) 85: 805-812, 2016.
18. Choi W, Li Y, Ji YS and Yoon KC: Oxidative stress markers in tears of patients with Graves' orbitopathy and their correlation with clinical activity score. BMC Ophthalmol 18: 303, 2018.
19. Edina K, Marianne D, Simone E, Oberic A, Turck N and Hamedani M: Differential profiling of lacrimal cytokines in patients suffering from thyroid-associated orbitopathy. Sci Rep 8: 10792, 2018.
20. Matheis N, Grus FH, Breitenfeld M, Knych I, Funke S, Pitz S, Ponto KA, Pfeiffer N and Kahaly GJ: Proteomics differentiate between thyroid-associated orbitopathy and dry eye syndrome. Invest Opth Vis Sci 56: 2649-2656, 2015.
21. Chng CL, Seah LL, Yang M, Shen SY, Koh SK, Gao Y, Deng L, Tong L, Beuerman RW and Zhou L: Proteins calcium binding protein A4 (S100A4) and prolactin induced protein (PIP) are potential biomarkers for thyroid eye disease. Sci Rep 8: 16936, 2018.
22. Yang M, Chung Y, Lang S, Yawata N, Seah LL and Looi A: The tear cytokine profile in patients with active Graves' orbitopathy. Endocrine 59: 402-409, 2018.
23. Ji Y, Qian Z, Dong Y, Zhou H and Fan X: Quantitative morphometry of the orbit in Chinese adults based on a three-dimensional reconstruction method. J Anat 217: 501-506, 2010.
24. Schiffman RM, Christianson MD, Jacobsen G, Hirsch JD and Reis BL: Reliability and validity of the ocular surface disease index. Arch Ophthalmol 118: 615-621 2000.
25. Jiang L and Wei R: Analysis of Graves' ophthalmopathy patients' tear protein spectrum. Chin Med J (Engl) 126: 4493-4498, 2013.
26. Breuer K, Foroushani AK, Laird MR, Chen C, Sribnaia A, Lo R, Winsor GL, Hancock RE, Brinkman FS and Lynn DJ: InnateDB: Systems biology of innate immunity and beyond-recent updates and continuing curation. Nucleic Acids Res 41 (Database Issue): D1228-D1233, 2013.
27. Jassal B, Matthews L, Viteri G, Gong C, Lorente P, Fabregat A, Sidiropoulos K, Cook J, Gillespie M, Haw R, *et al*: The reactome pathway knowledgebase. Nucleic Acids Res 48 (D1): D498-D503, 2020.
28. Haynes W: Benjamini-Hochberg Method. In: Dubitzky W, Wolkenhauer O, Cho KH and Yokota H (eds). Encyclopedia of Systems Biology. Springer, New York, NY, 2013.
29. Bautista EL: Inflammation, endothelial dysfunction, and the risk of high blood pressure: Epidemiologic and biological evidence. J Hum Hypertens 17: 223-230, 2003.
30. Haefliger IO, Von Arx G and Pimentel AR: Pathophysiology of intraocular pressure increase and glaucoma prevalence in thyroid eye disease: A mini-review. Klin Monbl Augenheilkd 227: 292-293, 2010.
31. Klein R, Klein BE, Knudtson MD, Wong TY and Tsai MY: Are inflammatory factors related to retinal vessel caliber? The beaver dam eye study. Arch Ophthalmol 124: 87-94, 2006.
32. Wall JR, Bernard N, Boucher A, Salvi M, Zhang ZG, Kennerdell J, Tyutyunikov A and Genovese C: Pathogenesis of thyroid-associated ophthalmopathy: An autoimmune disorder of the eye muscle associated with Graves' hyperthyroidism and Hashimoto's thyroiditis. Clin Immunol Immunopathol 68: 1-8, 1993.
33. Hwang CJ, Afifiyan N, Sand D, Naik V, Said J, Pollock SJ, Chen B, Phipps RP, Goldberg RA, Smith TJ and Douglas RS: Orbital fibroblasts from patients with thyroid-associated ophthalmopathy overexpress CD40: CD154 hyperinduces IL-6, IL-8, and MCP-1. Invest Ophthalmol Vis Sci 50: 2262-2268, 2009.
34. Hiromatsu Y, Yang D, Bednarczuk T, Miyake I, Nonaka K and Inoue Y: Cytokine profiles in eye muscle tissue and orbital fat tissue from patients with thyroid-associated ophthalmopathy. J Clin Endocrinol Metab 85: 1194-1199, 2000.
35. Wahrenberg H, Wennlund A and Hoffstedt J: Increased adipose tissue secretion of interleukin-6, but not of leptin, plasminogen activator inhibitor-1 or tumour necrosis factor alpha, in Graves' hyperthyroidism. Eur J Endocrinol 146: 607-611, 2002.
36. Kaback LA and Smith TJ: Expression of hyaluronan synthase messenger ribonucleic acids and their induction by interleukin-1beta in human orbital fibroblasts: Potential insight into the molecular pathogenesis of thyroid-associated ophthalmopathy. J Clin Endocrinol Metab 84: 4079-4084, 1999.
37. Khong JJ, McNab AA, Ebeling PR, Craig JE and Selva D: Pathogenesis of thyroid eye disease: Review and update on molecular mechanisms. Br J Ophthalmol 100: 142-150, 2016.
38. Ma R, Ren H, Xu B, Cheng Y, Gan L, Zhang R, Wu J and Qian J: PH20 inhibits TGFβ1-induced differentiation of perimysial orbital fibroblasts via hyaluronan-CD44 pathway in thyroid-associated ophthalmopathy. Invest Ophthalmol Vis Sci 60: 1431-1441, 2019.
39. Areschoug T and Gordon S: Scavenger receptors: Role in innate immunity and microbial pathogenesis. Cell Microbiol 11: 1160-1169, 2009.
40. Anderson CK and Miller OF III: Triad of exophthalmos, pretibial myxedema, and acropachy in a patient with Graves' disease. J Am Acad Dermatol 48: 970-972, 2003.
41. Esteban JA: AMPA receptor trafficking: A road map for synaptic plasticity. Mol Interv 3: 375-385, 2003.
42. Fowler JH, Mccracken E, Dewar D and McCulloch J: Intracerebral injection of AMPA causes axonal damage in vivo. Brain Res 991: 104-112, 2003.
43. Nellgård B and Wieloch T: Postischemic blockade of AMPA but not NMDA receptors mitigates neuronal damage in the rat brain following transient severe cerebral ischemia. J Cereb Blood Flow Metab 12: 2-11, 1992.
44. Wu LQ, Mou P, Chen ZY, Cheng JW, Le QH, Cai JP and Wei RL: Altered corneal nerves in chinese thyroid-associated ophthalmopathy patients observed by in vivo confocal microscopy. Med Sci Monit 25: 1024-1031, 2019.
45. Koga M, Hiromatsu Y, Jimi A, Inoue Y and Nonaka K: Possible involvement of Fas-mediated apoptosis in eye muscle tissue from patients with thyroid-associated ophthalmopathy. Thyroid 8: 311-318, 1998.
46. Zoukhri D, Fix A, Alroy J and Kublin CL: Mechanisms of murine lacrimal gland repair after experimentally induced inflammation. Invest Ophthalmol Vis Sci 49: 4399-4406, 2008.
47. Humphreys-Beher MG, Peck AB, Dang H and Talal N: The role of apoptosis in the initiation of the autoimmune response in Sjögren's syndrome. Clin Exp Immunol 116: 383-387, 1999.
48. Zoukhri D: Mechanisms involved in injury and repair of the murine lacrimal gland: Role of programmed cell death and mesenchymal stem cells. Ocul Surf 8: 60-69, 2010.
49. Smith TJ, Kahaly GJ, Ezra DG, Fleming JC, Dailey RA, Tang RA, Harris GJ, Antonelli A, Salvi M, Goldberg RA, *et al*: Teprotumumab for thyroid-associated ophthalmopathy. N Engl J Med 376: 1748-1761. 2017.